Article

Wildfire CO$_2$ Emissions in the Conterminous United States from 2015 to 2018 as Estimated by the WRF-Chem Assimilation System from OCO-2 XCO$_2$ Retrievals

Jiuping Jin [1], Qinwei Zhang [2], Chong Wei [1], Qianrong Gu [1] and Yongjian Huang [1,*]

[1] Shanghai Carbon Data Research Center, Key Laboratory of Low-Carbon Conversion Science & Engineering, Shanghai Advanced Research Institute, Chinese Academy of Sciences, Shanghai 201210, China; jinjp@sari.ac.cn (J.J.); weic@sari.ac.cn (C.W.)

[2] Sungrow Power Shanghai Company Limited, Shanghai 201107, China; zhangqinwei@sungrowpower.com

[*] Correspondence: huangyj@sari.ac.cn

Abstract: Wildfires are becoming more frequent due to the global climate change. Large amounts of greenhouse gases emitted by wildfires can lead to increases in extreme climate events. Accurately estimating the greenhouse gas carbon dioxide (CO$_2$) emissions from wildfires is important for mitigation of climate change. In this paper, we develop a novel method to estimate wildfire CO$_2$ emissions from the relationship between local CO$_2$ emissions and XCO$_2$ anomalies. Our method uses the WRF-Chem assimilation system from OCO-2 XCO$_2$ retrievals which coupled with Data Assimilation Research Testbed (DART). To validate our results, we conducted three experiments evaluating the wildfire CO$_2$ emissions over the conterminous United States. The four-month average wildfire emissions from July to October in 2015~2018 were estimated at 4.408 Tg C, 1.784 Tg C, 1.514 Tg C and 2.873 Tg C, respectively. Compared to the average of established inventories CT2019B, FINNv1.5 and GFASv1.2 fire emissions, our estimates fall within one standard deviation, except for 2017 due to lacking of OCO-2 XCO$_2$ retrievals. These results suggest that the regional carbon assimilation system, such as WRF-Chem/DART, using OCO-2 XCO$_2$ retrievals has a great potential for accurately tracking regional wildfire emissions.

Keywords: wildfire; CO$_2$ emissions; WRF-Chem/DART; assimilation system; the conterminous United States

1. Introduction

Wildfires occurring either naturally or ignited by humans are an important component of the global carbon cycle. It emits a variety of greenhouse, reactive gases and aerosols to the atmosphere, including carbon dioxide (CO$_2$), carbon monoxide (CO), oxides of nitrogen (NO$_x$), methane (CH$_4$), volatile and semivolatile organic compounds (VOC and SVOC), particulate matter (PM), ammonia (NH$_3$), sulfur dioxide (SO$_2$) and so on. This not only cause the immediate release of carbon stored in vegetation into the atmosphere, but also induce a long-term shift in the balance between the carbon sequestration by plants and carbon liberation through decomposition of dead biomass. This will affect the atmospheric composition and thermal balance in both the global and regional scales [1–6]. In recent decades, varying degrees of wildfires happened now and then in Australia, California, Siberia and Indonesia. These wildfires had a significant impact on the ecological environment, human health, and economic life in these regions [7–10]. Wang et al. [11] use a combination of physical, epidemiological and economic models to estimate the economic impacts of California wildfires in 2018. The estimation result shows that the wildfire damages in 2018 totaled $148.5 (126.1–192.9) billion (roughly 1.5% of California's annual gross domestic product).

Wildfires affect climate through direct carbon dioxide CO$_2$ emissions and multiple postfire carbon source and sink pathways. Globally, since 2000, CO$_2$ emissions from fossil

fuels and land-use change averaged 9 billion metric tons of carbon (Gt C) per year, whereas wildfire CO_2 emissions were approximately 2 Gt C per year [12]. Over the past few decades, the increasing frequency of wildfires is a concerning trend that is linked to the global warming [13]. In the conterminous United States, the increase in burned area from wildfires has roughly quadrupled. This trend is concerning because wildfires can contribute to the accumulation of greenhouse gases in the atmosphere, which in turn leads to further global warming. Many studies have analyzed various aspects of the atmospheric impacts of wildfires, ranging from the more general such as air quality issue and emissions assessment, to more specific or local including particulate matter emissions, transport, radiative effects and so on [14]. Miranda et al. [15] estimated CO_2 emissions due to wildfires and found that in years when the burnt area exceeds 100000ha, this contribution could reach 7% of the total Portuguese CO_2 emissions. So, it is important to study the variation of wildfire CO_2 emissions on both global and regional scales which will improve our understanding of the damage from wildfires. The analysis of wildfires CO_2 emissions can provide a valuable foundation for decision-makers to formulate relevant policies.

The variety of satellites and observation data provide conveniences for the estimation of the wildfire CO_2 emissions scale and the real-time monitoring of fire points [16–19]. Different research groups produced the wildfire CO_2 emissions dataset such as Global Fire Emission Database (GFED) [20,21], Fire INventory from NCAR (FINN) [22], Global Fire Assimilation System (GFAS) [23] by using the burning area (BA) and fire radiative power (FRP). Where the FRP observed by satellite data such as Moderate Resolution Imaging Spectroradiometer (MODIS). Konovalov et al. [24] propose a method to estimate the wildfires CO_2 emissions in Siberia. This method use Infrared Atmospheric Sounding Interferometer (IASI) carbon monoxide (CO) retrievals and MODIS Aerosol Optical Depth (AOD) combined with outputs from the CHIMERE mesoscale chemistry-transport model. The study found the "top-down" estimates for the total annual biomass burning CO_2 emissions in the period from 2007 to 2011 in Siberia are by factors of 2.5 and 1.8 larger than the respective bottom-up estimates, such as GFED3.1 and GFASv1.0 global emission inventories. Heymann et al. [25] estimate the Indonesian fire CO_2 emissions by using the column-averaged dry air mole fraction of CO_2 (XCO_2) which derived from measurements of the Orbiting Carbon Observatory-2 (OCO-2) satellite mission. The estimated wildfire CO_2 emissions is 748 ± 209 Mt CO_2, which is about 30% lower than GFEDv4s and GFASv1.2. Guo et al. [26,27] successively evaluated the CO_2 emissions from the 2010 fires in western Russia by using Greenhouse Gases Observing Satellite (GOSAT) data, from the 2015 fires in Siberia by using OCO-2 data. Wang et al. [28] studies the 2019–2020 Australian mega-bushfires based on OCO-2 XCO_2 retrievals. Find the smoke from wildfires can greatly obscure satellite observations, making the available XCO_2 mainly locate over outer fringes of plumes downwind of the major mega-bushfires in eastern Australia in three orbit observations during November-December 2019 with their enhancements of approximately 1.5 ppm. By using an atmospheric transport model, the fire-induced CO_2 enhancement is further confirmed. The simulation experiment also suggests that the sensitivity of the downwind maximum XCO_2 enhancement is 0.41 ± 0.04 ppm for 1 Tg C d^{-1} fire emissions.

In this paper, we assess the wildfire CO_2 emissions in conterminous United States from July to October in 2015~2018 with the regional CO_2 assimilation inversion system [29]. It can improve the regional CO_2 concentrations by assimilating OCO-2 XCO_2 retrievals with WRF-Chem coupled with extending the DART [30]. We evaluate our results with CT2019B, FINNv1.5 and GFASv1.2 wildfire emissions databases.

The paper is organized as follows, the detail description of the estimate method and materials are presented in the Section 2; Results of the experiments and discussion are given in Section 3, followed by the conclusion in Section 4.

2. Materials and Methods

2.1. A Regional CO_2 Transport Model

WRF-Chem model version 4.4 was used as regional CO_2 transport model. The study area is the conterminous United States, the time range is from July to October in 2015~2018. The physics and chemistry configurations of WRF-ChemV4.4 is showed in Table 1 [29].

Table 1. Physics and chemistry configurations of the WRF-Chem V4.4.

Options	Configurations
WRF_Core	ARW
Domain center	34.939°N–96.275°W
Grid resolution	50 km
nx,ny,nz	103,82,45
Interval seconds	21,600 s/6 h
Time steps	240 s
Start date	2015~01-07-2018 00:00:00
End date	2015~01-11-2018 00:00:00
Microphysics process	WSM 5-class simple ice scheme [31]
Cumulus parameterization	Kain-Fritsch scheme [32]
Longwave atmospheric radiation	RRTM scheme [33]
Shortwave atmospheric radiation	Dudhia scheme [34]
Planetary boundary layer scheme	MYNN 2.5 level TKE [35]
Surface layer scheme	MYNN [36]
Land surface scheme	Unified Noah Land surface model
Chemistry option	chem_opt=16 (CO_2 only)

The WRF-Chem model use ds083.2 data (DOI: 10.5065/D6M043C6) as the initial meteorological dataset, which is $1° \times 1°$ spatial resolution and 6-hourly temporal resolution from National Centers for Environmental Prediction (NCEP) FNL Operational Model Global Tropospheric Analyses, continuing from July 1999.

The initial and boundary conditions of CO_2 concentrations on WRF-Chem model are interpolated from CT2019B CO_2 total mole fractions products which is $3° \times 2°$ spatial resolution and three-hourly temporal resolution. The prior CO_2 flux is CT2019B flux which is $1° \times 1°$ spatial resolution and three-hourly temporal resolution, including anthropogenic emissions, fire emissions, biogenic fluxes, and ocean fluxes.

2.2. CO_2 Concentration Assimilation System

The study is based on the regional CO_2 concentration assimilation system with OCO-2 XCO_2 retrievals by extending DART [29,30].

The XCO_2 retrievals from nadir observation mode with good quality according to the "xco2_quality_flag" are selected from the OCO-2 Level2 (L2) Lite data product V10 and its preprocessing method is as below [29]:

$$\widetilde{OCO2_{XCO_2}} = \sum_{i=1}^{n} OCO2_{XCO_{2i}} \sigma_{OCO2_i}^{-2} / \sum_{i=1}^{n} \sigma_{OCO2_i}^{-2} \tag{1}$$

$$\widetilde{\sigma_{OCO2}} = 1 / \sqrt{N^{-1} \sum_{i=1}^{n} \sigma_{OCO2_i}^{-2}} \tag{2}$$

where $\widetilde{OCO2_{XCO_2}}$ and $\widetilde{\sigma_{OCO2}}$ denotes the representative mean XCO_2 value and its uncertainty of a model grid cell respectively.

According to the strategy of Crowell et al. [37], the observation operator H was implemented to link the OCO-2 10 s mean XCO_2 retrievals to the CO_2 concentration forecast by WRF-Chem model, which is defined as:

$$XCO_2^m = XCO_2^a + \sum_j h_j a_j (CO_2^m - CO_2^a) \tag{3}$$

where XCO_2^a, h_j, a_j and CO_2^a are the prior XCO_2 value, the pressure weighting function, the column averaging kernel and the prior CO_2 concentration profile used by OCO-2 XCO_2 retrieval process respectively. CO_2^m is the optimal CO_2 concentration profile which interpolated to the pressure levels of OCO-2 XCO_2 retrieval from WRF-Chem model. XCO_2^m is the column-average CO_2 concentration of the WRF-Chem forecasts which converted by the operator H.

The assimilation system used Ensemble Adjustment Kalman Filter (EAKF) [38] as the data assimilation approach, and advanced by WRF-Chem to next assimilation cycle. Let x_k^{init}, x_k^f, x_k^a represent the initial states of the prior CO_2 concentration distribution, the forecast states advanced by WRF-Chem starting from x_k^{init} and the analysis states of the k-th ensemble member of each assimilation cycle, respectively. The x_k^{init} was generated in the same way as that of Mizzi et al. [39] by imposing a Gaussian distribution around mean values of CO_2 concentrations calculated from CT2019B as the initial background with a 5% standard deviation about the mean. The forecast states x_k^f were transformed into the observation space by the observation operator H, i.e., $y_{m,k}^f = H(x_k^f)$, where the subscript m means "from model". The analysis result of each $y_{m,k}^f$ was calculated as:

$$y_{m,k}^a = \left[\sqrt{\frac{\widetilde{\sigma_{OCO2}}^2}{\widetilde{\sigma_{OCO2}}^2 + \bar{\sigma}_m^{f2}}} \right] \left[y_{m,k}^f - \bar{y}_m^f \right] + \left[\frac{\bar{y}_m^f}{\bar{\sigma}_m^{f2}} + \frac{\widetilde{OCO2}_{XCO_2}}{\widetilde{\sigma_{OCO2}}^2} \right] \left[\frac{1}{\bar{\sigma}_m^{f2}} + \frac{1}{\widetilde{\sigma_{OCO2}}^2} \right]^{-1} \tag{4}$$

where $\widetilde{OCO2}_{XCO_2}$ is the representative mean XCO_2 values of a model grid cell with uncertainty $\widetilde{\sigma_{OCO2}}$ calculated from the OCO-2 retrievals by Equations (1) and (2). $\bar{y}_m^f$ is the ensemble forecast mean with ensemble spread $\bar{\sigma}_m^{f2}$ in the observation space. At the end of each assimilation cycle, the analysis state of the k-th ensemble member was updated as:

$$x_k^a = x_k^f + \alpha \frac{\sigma(x^f, y_m^f)}{\bar{\sigma}_m^{f2}} (y_{m,k}^a - y_{m,k}^f) \tag{5}$$

where $\sigma(x^f, y_m^f)$ is the covariance of x^f and y_m^f across the ensemble. α is a covariance localization function to compensate the sampling error due to small ensemble size [40].

2.3. Wildfire Emissions Estimate Model

Hakkarainen et al. [41,42] indicates a positive correlation between XCO_2 anomalies and CO_2 emission inventories in regional-scale, which can be defined as:

$$\Delta F = \lambda * \Delta XCO_2 \tag{6}$$

where ΔF is CO_2 emissions, ΔXCO_2 is the XCO_2 anomalies corresponding to CO_2 emissions, λ is the positive correlation coefficient.

We propose a model to estimate the wildfire CO_2 emissions in the conterminous United States. First we design two simulation experiments to compute the positive correlation coefficient λ. The difference between two simulation experiments is whether to add the wildfire emissions to the prior flux or not. Where the ΔXCO_2 is the XCO_2 anomalies derived from the two simulation experiments results. ΔF is the wildfire CO_2 emissions. Then we design one CO_2 assimilation experiment to estimate the wildfire emissions in conterminous United States with the known coefficient λ and XCO_2 anomalies. So, we obtain an equation about CO_2 emissions increment and XCO_2 increment in the wildfire area, which defined as follows:

$$\frac{\Delta Flux1}{\Delta XCO2\_1} = \frac{\Delta Flux2}{\Delta XCO2\_2} \tag{7}$$

where $\Delta Flux1$ and $\Delta Flux2$ represent two CO_2 flux increment respectively, the $\Delta XCO2\_1$ and $\Delta XCO2\_2$ are the XCO_2 increment corresponding to the above two CO_2 flux increment.

2.4. Wildfire Emissions of CT2019B

By analyzing the CT2019B monthly total CO_2 fluxes, anthropogenic CO_2 emissions, biological CO_2 fluxes, fire CO_2 emissions and ocean CO_2 fluxes from 2000 to 2018 in conterminous United States, we found the monthly mean anthropogenic CO_2 emissions does not change significantly with time, while the monthly mean biogenic CO_2 fluxes has obvious seasonal and inter-annual changes.

In the total CO_2 fluxes, the proportion of wildfire CO_2 emissions is less than 7%. Large-scale wildfires typically occurred in summer, particularly in August and September, and this trend has been increasing year by year from 2000 to 2018. As Figure 1 shows, in the year 2015∼2018, the wildfires occurred in July and August of each year mainly at northwest area of the conterminous United States, and the wildfire in August is larger than July. While in September and October the wildfire also appeared at southeast area of the conterminous United States.
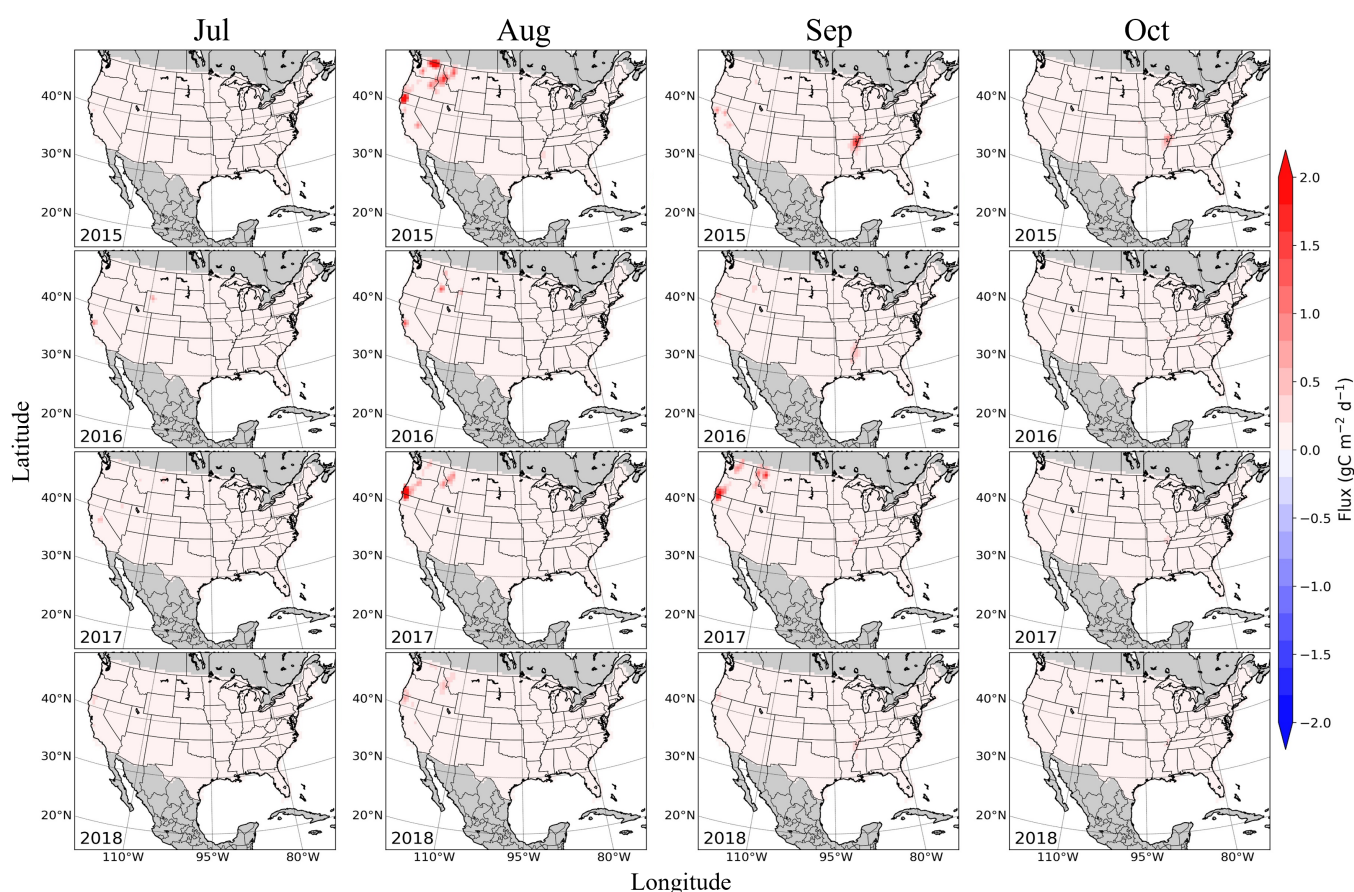

Figure 1. The spatial distribution of wildfire CO_2 emissions in July to October in conterminous United States during 2015 to 2018.

2.5. Experiment Design

In this paper, we design three groups of comparative experiments. Two CO_2 concentration simulation experiments named as "SIM_EXP1" and "SIM_EXP2", one CO_2 concentration assimilate experiment with the OCO-2 XCO_2 retrievals named as "DA_EXP3". The configurations of the three experiments are shown in Table 2.

Table 2. The configurations of the three experiments.

Experiment Name	Initial and Boundary	Prior Flux	Assimilate or Not	Experiment Time
SIM_EXP1	CT2019B CO_2 total mole fractions products	CT2019B optimized fluxes with fire emissions	NO	July to October of 2015~2018
SIM_EXP2	CT2019B CO_2 total mole fractions products	CT2019B optimized fluxes without fire emissions	NO	July to October of 2015~2018
DA_EXP3	CT2019B CO_2 total mole fractions products	CT2019B optimized fluxes without fire emissions	YES	July to October of 2015~2018

The two simulation experiments SIM_EXP1, SIM_EXP2 were designed to demonstrate the significant impact of wildfire emissions on XCO_2. For SIM_EXP1, the initial and boundary conditions of the WRF-Chem were interpolated from CT2019B CO_2 total mole fractions products, the prior CO_2 flux was interpolated from CT2019B total fluxes which include anthropogenic emissions, fire emissions, biogenic fluxes, and ocean fluxes. For SIM_EXP2, the initial and boundary conditions were the same as SIM_EXP1, but the prior CO_2 fluxes only include anthropogenic emissions, biogenic fluxes and ocean fluxes.

For DA_EXP3 experiment, we optimizing the CO_2 concentrations further by assimilating with OCO-2 XCO_2 retrievals [30,38,43]. The prior fluxes are same as SIM_EXP2. The initial and boundary conditions was interpolated from CT2019B CO_2 total mole fractions products, and then adding a Gaussian perturbation which the average value is 0, standard deviation is 2% to each grid point of each ensemble. In this CO_2 assimilation experiment, the size of ensemble members is set to 20, adopting Three-dimensional Gaspari-Cohn localization function [44] to compensate for sampling errors caused by the finite ensemble number. Where the influence radius in the horizontal of Three-dimensional Gaspari-Cohn localization function is 0.1 radians. In vertical, the principle of localization function is same as Kang et al. [45], which has a larger impact coefficient in lower troposphere (the sigma level of OCO-2 is 0.947) and descending to both sides. Simultaneously, we discard the observations that is 3 times larger than the prior value by implementing the exception value detection.

2.6. Wildfire Emissions Estimate Method

According to the three experiments results, the Equation (7) can be rewrite as:

$$\frac{\Delta F_{exp1-exp2}}{X_{exp1} - X_{exp2}} = \frac{\Delta F_{wildfire}}{X_{exp3} - X_{exp2}} \tag{8}$$

where the X_{exp1}, X_{exp2} and X_{exp3} are the mean XCO_2 of SIM_EXP1, SIM_EXP2 and DA_EXP3. $\Delta F_{exp1-exp2}$ represents the CT2019B wildfire CO_2 emissions between SIM_EXP1 and SIM_EXP2, $\Delta F_{wildfire}$ is the estimated wildfire emissions in conterminous United States from our study.

To estimate the wildfire emissions accurately, we add the monthly ratio of wildfire emissions with OCO-2 XCO_2 retrievals days as a variable. Let i represent one month, $D^i_{wildfire}$ represent the days of wildfire occurs in one month, D^i_{total} represent total days of one month. Then the monthly ratio ρ^i defined as:

$$\rho^i = \frac{D^i_{wildfire}}{D^i_{total}} \tag{9}$$

The estimated wildfire CO_2 emissions $\Delta F^i_{wildfire}$ can be computed as:

$$\Delta XCO2\_1^i = X^i_{exp1} - X^i_{exp2} \tag{10}$$

$$\Delta XCO2\_2^i = X^i_{exp3} - X^i_{exp2} \tag{11}$$

$$\Delta F^i_{wildfire} = \Delta F^i_{exp1-exp2} \times \frac{\Delta XCO2\_2^i}{\Delta XCO2\_1^i} \times \rho^i \tag{12}$$

2.7. Evaluation Data

Three different types of wildfire CO_2 emissions were used to evaluate the wildfire CO_2 emissions in conterminous United States which estimated by our method. Including CT2019B fire emissions, CAMS GFASv1.2 wildfire CO_2 emissions datasets (https://ads.atmosphere.copernicus.eu/cdsapp#!/dataset/cams-global-fire-emissions-gfas?tab=overview, accessed on 15 November 2023) [46,47] with $0.1° \times 0.1°$ spatial resolution and FINNv1.5 fire emissions (https://www.acom.ucar.edu/Data/fire/, accessed on 15 November 2023) [22].

In our study, we also consider the influence of OCO-2 XCO_2 retrievals in wildfire areas. Before evaluating the wildfire CO_2 emissions based on the Equations (10)–(12), it is necessary to select the days with sufficient OCO-2 XCO_2 retrievals in wildfire areas. Table 3 shows the selected days in conterminous United States from July to October of 2015~2018. As there are no OCO-2 XCO_2 retrievals in August 2017, the number of days that can be selected is zero.

Table 3. The OCO-2 XCO_2 observations days in wildfire areas of the conterminous United States from July to October of 2015~2018.

Year	July	August	September	October
2015	9	8	8	6
2016	6	7	10	10
2017	12	0	3	6
2018	10	14	18	18

The CT2019B CO_2 concentrations and NCEP Reanalysis2 Gaussian Grid 10 m wind data were used to analysis the variation of wildfire CO_2 emissions in the conterminous United States.

2.8. Evaluation Metrics

Our experiments results were evaluated by Standard Deviation (STDE), defined as:

$$STDE = \sqrt{\frac{\sum_{i=1}^{n}(f_i - \bar{f})^2}{n - 1}} \tag{13}$$

where n is the 3, means the three kinds of wildfire emissions as mentioned in Section 2.7. f_i represent one of the three types of wildfire emissions. $\bar{f}$ is the averaged wildfire emissions of CT2019B, GFASv1.2, FINNv1.5.

3. Results and Discussion

3.1. XCO_2 Experiments Results

Table 4 shows the monthly average XCO_2 of SIM_EXP1, SIM_EXP2, DA_EXP3 and CT2019B from July to October of 2015~2018 in conterminous United States, with the CT2019B XCO_2 added as reference. As the Table 4 shows, the average annual increase in XCO_2 is approximately 2.57 ppm for the three experiments. The monthly averaged XCO_2

exhibits an uptrend from August to October every year, especially in October, where XCO_2 increases by 1.47 ppm, 1.27 ppm, 1.45 ppm, 1.11 ppm from 2015 to 2018 respectively.

Due to the absence of wildfire emissions in the prior fluxes of WRF-ChemV4.4 model, the monthly averaged XCO_2 of SIM_EXP2 is 0.02ppm lower than SIM_EXP1 in conterminous United States. The monthly averaged XCO_2 of DA_EXP3 is closer to CT2019B than SIM_EXP1 and SIM_EXP2, indicating the assimilation of OCO-2 XCO_2 retrievals can optimize the XCO_2 distribution and make it more consistent with the CarbonTracker products.

Table 4. The monthly average XCO_2 of SIM_EXP1, SIM_EXP2, DA_EXP3 and CT2019B from July to October of 2015~2018 in conterminous United States.

Year	Month	SIM_EXP1 (ppm)	SIM_EXP2 (ppm)	DA_EXP3 (ppm)	CT2019B (ppm)
2015	July	398.60	398.58	398.22	398.29
	August	397.13	397.09	396.59	396.65
	September	397.67	397.65	397.61	397.36
	October	399.19	399.18	398.98	398.81
2016	July	402.06	402.06	401.41	401.86
	August	401.13	401.12	400.49	400.51
	September	401.22	401.21	401.12	400.77
	October	402.45	402.45	402.46	402.07
2017	July	404.77	404.76	403.69	404.21
	August	402.49	402.47	401.52	402.05
	September	402.97	402.95	403.01	402.45
	October	404.43	404.43	404.41	404.01
2018	July	405.83	405.82	405.39	405.61
	August	405.12	405.07	404.67	404.80
	September	405.68	405.66	405.56	405.21
	October	406.74	406.73	406.75	406.28

3.2. Wildfire CO_2 Emissions Experiments Results

Due to satellite transit time, clouds and aerosols, OCO-2 satellite only has several days in which it can detect wildfire in conterminous United States from July to October. To accurately estimate monthly wildfire CO_2 emissions, the days we selected are those with OCO-2 XCO_2 retrievals coupled with wildfires.

Figure 2 shows the spatial distribution of monthly mean CT2019B wildfire CO_2 emissions with 10m wind speed and wind direction in upper panel, the monthly mean ΔXCO_2 between DA_EXP3 and SIM_EXP2 with sufficient OCO-2 XCO_2 retrievals days in lower panel, the time range is from July to October in 2015~2018.

As the Figure 2 shows, compared with SIM_EXP2, after assimilating with OCO-2 XCO_2 retrievals, the XCO_2 increment of DA_EXP3 mainly locate in or around the wildfire areas. Taking into account the distribution and numeric value of the OCO-2 XCO_2 retrievals, the range of wildfire occurrences in the conterminous United States, the 10m wind speed and wind direction in different months and the CO_2 assimilate system, the XCO_2 increment is primarily located in the north and east, and SIM_EXP2 having a larger XCO_2 than DA_EXP3 in the other regions in July and August. In September and October, the XCO_2 increment mainly locate in northwest and southeast regions where the wildfire occurs, and the negative value of ΔXCO_2 is less than July and August.
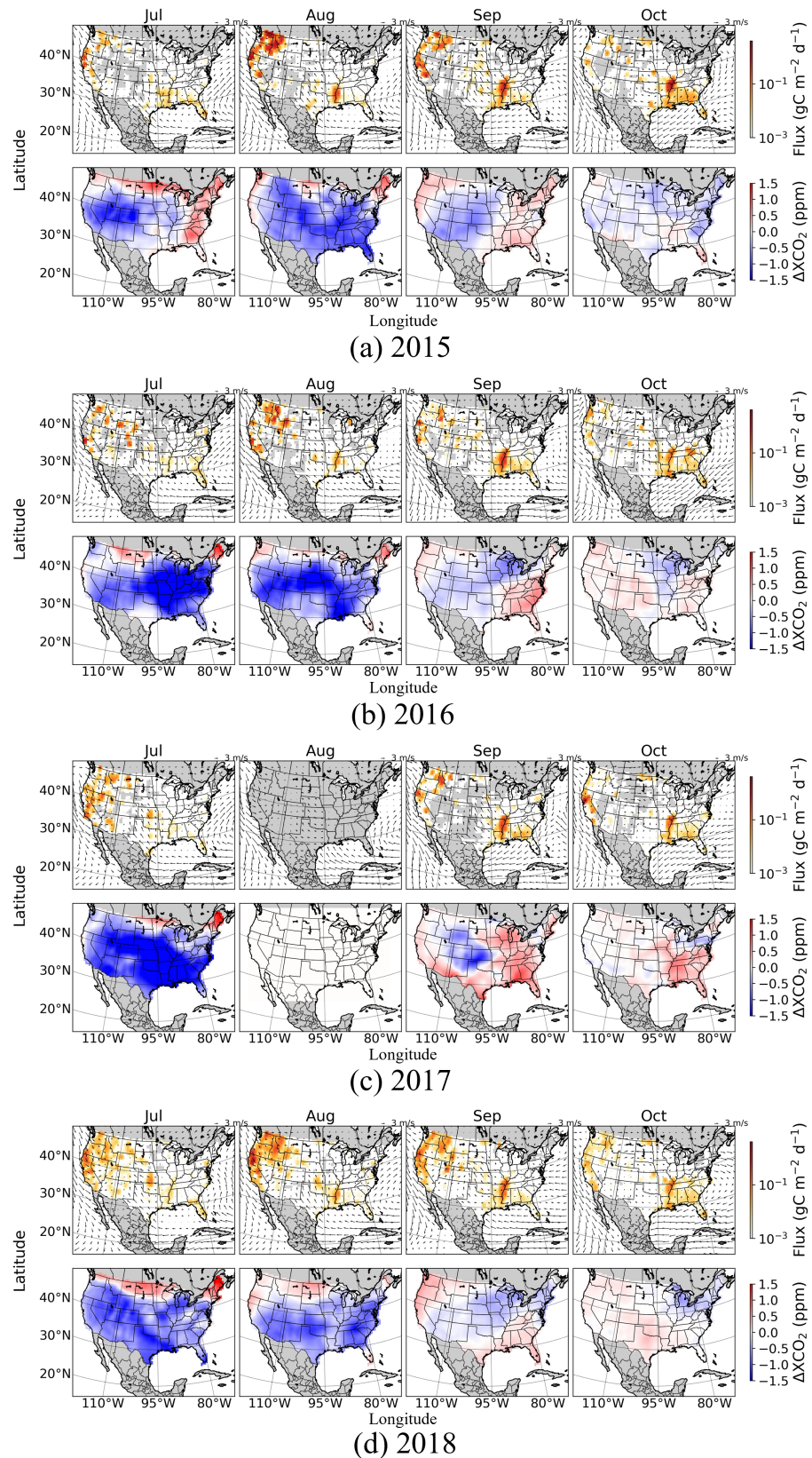
Figure 2. The spatial distribution of monthly mean wildfire CO_2 emissions from CT2019B with the 10m wind speed and wind direction in the conterminous United States (**upper panel**), the monthly mean ΔXCO_2 between DA_EXP3 and SIM_EXP2 with enough OCO-2 XCO_2 observations in the conterminous United States (**lower panel**), the time range is from July to October in 2015~2018.

Figure 3 shows the comparison between mean wildfire CO_2 emissions of CT2019B, FINNv1.5, GFASv1.2 and estimates in our study. The monthly mean wildfire emissions of CT2019B, FINNv1.5, GFASv1.2 and our study are presented in Table 5. In our study, the four-month mean wildfire emissions in 2015 are 4.408 Tg C (1 Tg C = 10^{12} g C), which is 26.34% higher than CT2019B, 33.63% higher than FINNv1.5 and 24.47% lower than GFASv1.2. These values fall within one standard deviation of the average values of CT2019B, FINNv1.5 and GFASv1.2 (4.208 ±2.082 Tg C).

The four-month mean wildfire emissions in 2016 is 1.784 Tg C, is 34.05% larger than CT2019B, 32.26% lower than FINNv1.5 and 55.45% lower than GFASv1.2. While in 2017, because of the lack of OCO-2 observation data in August and September, the evaluation of wildfire emissions with our study is inaccurate, the four-month mean wildfire emissions of our study have a large gap with the other three emissions databases. And the four-month mean wildfire emissions in 2018 is 2.873 Tg C, is 53.72% larger than CT2019B, 35.29% lower than FINNv1.5 and 44.12% lower than GFASv1.2, which also falls within one standard deviation of the average of other three wildfire emissions.

The differences in wildfire CO_2 emissions between different data sources are significant for each month. For instance, in August 2015, the wildfire CO_2 emissions of GFASv1.2 are 18.391 Tg C, where those of FINNv1.5 are 7.238 Tg C. In October 2015, the wildfire CO_2 emissions in our study are 4.263 Tg C, higher than all the others. The similar phenomenon also occurred in 2016~2018, and the gap may be caused by the different estimation methods, model errors, different CO_2 satellites observation data and so on. For example, GFAS use the top-down approach to calculate the biomass burning emissions by assimilating FRP observations from the MODIS instruments onboard the Terra and Aqua satellites. It corrects the gaps in the observations, considers the omission errors due to the undetected small fires, using atmospheric reactive gas simulations to produce the real time daily, $0.5° \times 0.5°$ grid, global wildfire emissions. But the occurrence of a plume may be wrongly predicted or not predicted at all in situations with extreme variability in the fire activity. FINN use the bottom-up approach to provide daily, 1 km resolution, global estimates of emissions from open fires based on the Terra and Aqua from MODIS instruments satellite detection of hot spots. This method mainly uses the fire hot spots to estimate the wildfire emissions, ignoring the impact of smaller fires on CO_2 emissions. And the use of assumed area burned, land cover maps, biomass consumption estimates, and emission factors all will introduce error into the model estimates. This leads to highly underestimation of the fire emissions in global, then causing the uncertainties and the large fluctuations in regional. CarbonTracker provides 3-hourly, $1° \times 1°$ grid, global estimates of surface-atmosphere CO_2 fluxes. For fire emissions, it uses GFED as one of the fire modules to estimate biomass burning. The burned area is based on MODIS satellite observations of fire counts, together with detailed vegetation cover information and a set of vegetation specific scaling factors. Based on the burned area estimate, the seasonally changing vegetation and soil biomass stocks in the CASA model are combusted and converted to atmospheric trace gases using estimates of fuel loads, combustion completeness, and burning efficiency. The diversity of wildfire CO_2 emissions estimation methods will induce the difference in estimation results, but it also promotes the progress of the estimation methods.
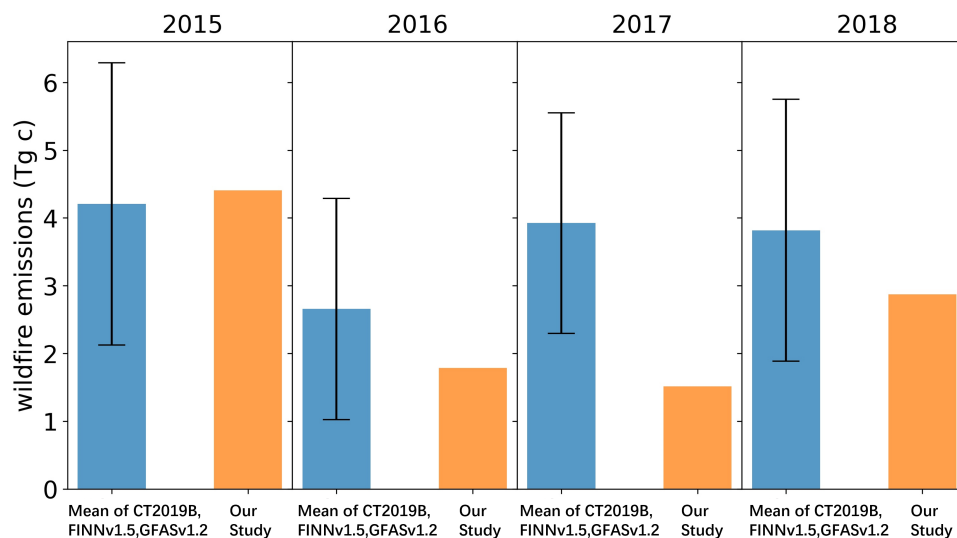
Figure 3. The comparison between mean wildfire CO_2 emissions of CT2019B, FINNv1.5, GFASv1.2 and our study in the conterminous United States from July to October in 2015~2018.

Table 5. The wildfire CO_2 emissions of CT2019B, FINNv1.5, GFASv1.2 and our study in the conterminous United States from July to October in 2015~2018.

Year	Wildfire Emissions(Tg C)	July	August	September	October	Mean
2015	CT2019B	0.537	8.614	3.356	1.450	3.489
	FINNv1.5	1.840	7.238	1.872	2.246	3.299
	GFASv1.2	1.154	18.391	1.319	2.481	5.836
	Mean of CT2019B, FINNv1.5,GFASv1.2	1.177 ± 0.652	11.414 ± 6.081	2.182 ± 1.053	2.059 ± 0.541	4.208 ± 2.082
	Our study	3.568	8.251	1.552	4.263	4.408
2016	CT2019B	0.875	1.729	1.765	0.954	1.331
	FINNv1.5	1.827	2.506	2.725	3.475	2.633
	GFASv1.2	4.341	6.714	3.269	1.693	4.004
	Mean of CT2019B, FINNv1.5,GFASv1.2	2.348 ± 1.791	3.650 ± 2.682	2.586 ± 0.761	2.041 ± 1.296	2.656 ± 1.633
	Our study	0.511	0.791	3.999	1.834	1.784
2017	CT2019B	1.202	4.204	4.622	1.210	2.810
	FINNv1.5	1.553	4.664	6.629	3.949	4.199
	GFASv1.2	6.803	3.317	6.982	1.966	4.767
	Mean of CT2019B, FINNv1.5,GFASv1.2	3.186 ± 3.137	4.062 ± 0.685	6.078 ± 1.273	2.375 ± 1.415	3.925 ± 1.627
	Our study	1.758	NA	0.733	2.052	1.514
2018	CT2019B	1.556	3.568	1.620	0.733	1.869
	FINNv1.5	3.905	7.771	2.918	3.168	4.441
	GFASv1.2	6.071	8.340	4.803	1.354	5.142
	Mean of CT2019B, FINNv1.5,GFASv1.2	3.844 ± 2.258	6.560 ± 2.607	3.114 ± 1.600	1.752 ± 1.265	3.817 ± 1.933
	Our study	2.087	3.061	4.100	2.246	2.873

3.3. Effect of OCO-2 XCO₂ Retrievals
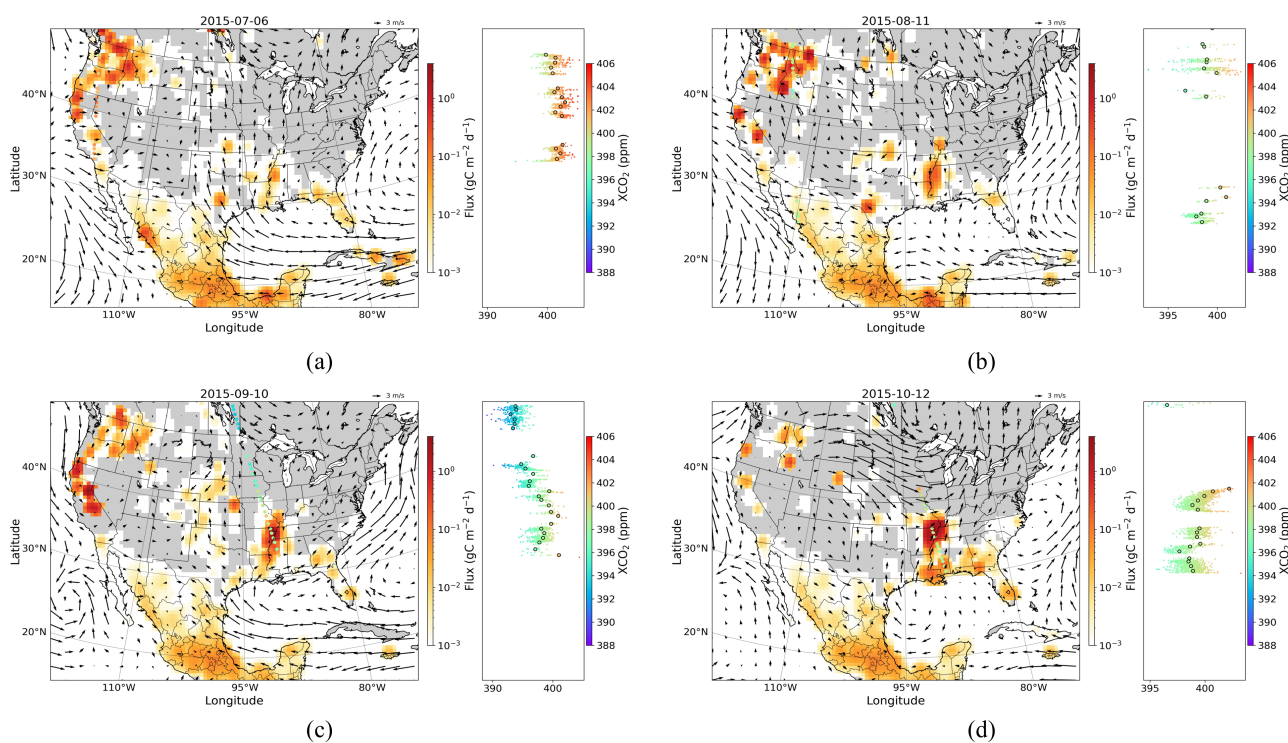
For each subgraph of Figure 4, the left panel shows the spatial distribution of CT2019B wildfire emissions with 10m wind speed and wind direction, and the 10s averaged OCO-2 XCO_2 retrievals with nadir mode, the right panel shows the latitude variation of 10s average OCO-2 XCO_2 retrievals with nadir mode.

As the Figure 4a shows, the massive wildfire occurs in the northwest area of the conterminous United States, accompanied by north winds near the OCO-2 observation area. Taking the observations of the northernmost in the wildfire area as the background value,

the maximum increment of OCO-2 XCO_2 retrievals is about 5.17 ppm. In Figure 4b, a larger wildfire occurs in northwest region, but that day has south winds. Using observations from southernmost in the wildfire area as the background value, the maximum increment of OCO-2 XCO_2 retrievals is approximately 3.16 ppm. In Figure 4c, the wildfire occurs in northwest and southeast region, but the OCO-2 observations mainly located in the center by southeast accompanied by north wind, the OCO-2 observations have an obvious upward trend in the southeast where the wildfire area, the maximum increment of OCO-2 XCO_2 retrievals is about 3.92 ppm. In Figure 4d, the wildfire mainly occurs in southeast region, accompanied by southwest wind, the maximum increment of OCO-2 XCO_2 retrievals is about 1.91 ppm.

Figure 4. The spatial distribution of CT2019B wildfire CO_2 emissions with the 10m wind speed and wind direction, 10s average OCO-2 XCO_2 retrievals with nadir mode (**left panel**), the latitude variation of 10s average OCO-2 XCO_2 retrievals with nadir mode (**right panel**). **(a)** 6 July 2015; **(b)** 11 August 2015; **(c)** 10 September 2015; **(d)** 12 October 2015.

Then analysis the XCO_2 of DA_EXP3 with the same select days are shown in Figure 4. The daily average XCO_2 distribution of SIM_EXP1, SIM_EXP2, DA_EXP3 and ΔXCO_2 between them are shown in Figure 5. In Figure 5a, the average XCO_2 of SIM_EXP1, SIM_EXP2 and DA_EXP3 in the northwest area of conterminous United States are 398.193 ppm, 398.192 ppm, 398.673 ppm respectively. Comparing with SIM_EXP1 and SIM_EXP2, the XCO_2 increment of DA_EXP3 mainly locate in northwest region where wildfire occurs and northeast region where no wildfire. As Figure 4a shows the wildfire areas, the distribution of OCO-2 XCO_2 retrievals and the wind direction, The XCO_2 increment of northeast region may affect by the north wind in northwest region and west wind in southwest region.

In Figure 5b, the XCO_2 of SIM_EXP2 is smaller than SIM_EXP1 due to the lack of wildfire CO_2 emissions in the northwest of conterminous United States. After assimilating OCO-2 XCO_2 retrievals, the XCO_2 of DA_EXP3 has shown improvement in regions affected by wildfires. Compared to SIM_EXP2, the results are more aligned with those of SIM_EXP1. This suggests that assimilating OCO-2 XCO_2 retrievals are effective in correcting deviations

in CO_2 concentration that are caused by wildfire emissions. Besides, the XCO_2 distribution of DA_EXP3-SIM_EXP2 and DA_EXP3-SIM_EXP1 in other area of conterminous United States mainly due to the change of the initial CO_2 concentration in each assimilation cycle.

In Figure 5c, the difference of XCO_2 between SIM_EXP1 and SIM_EXP2 is small in the southeast of conterminous United States. After assimilation, the XCO_2 of DA_EXP3 in the east region increased by assimilate with OCO-2 XCO_2 retrievals, wind speed and wind direction (Figure 4c). However, the XCO_2 of DA_EXP3 in the middle region decreased due to the smaller OCO-2 XCO_2 retrievals in this area, and this phenomenon indicates that the wildfire CO_2 emissions in SIM_EXP1 may be underestimated.

In Figure 5d, the difference of XCO_2 between SIM_EXP1 and SIM_EXP2 is mainly in the southeast of conterminous United States where the wildfire occurs. Compared with the XCO_2 of DA_EXP3, the results of SIM_EXP1 and SIM_EXP2 are smaller in southwest and middle north region, but larger in southeast, this may be affected by atmospheric transmission, wind speed, wind direction and prior fluxes.
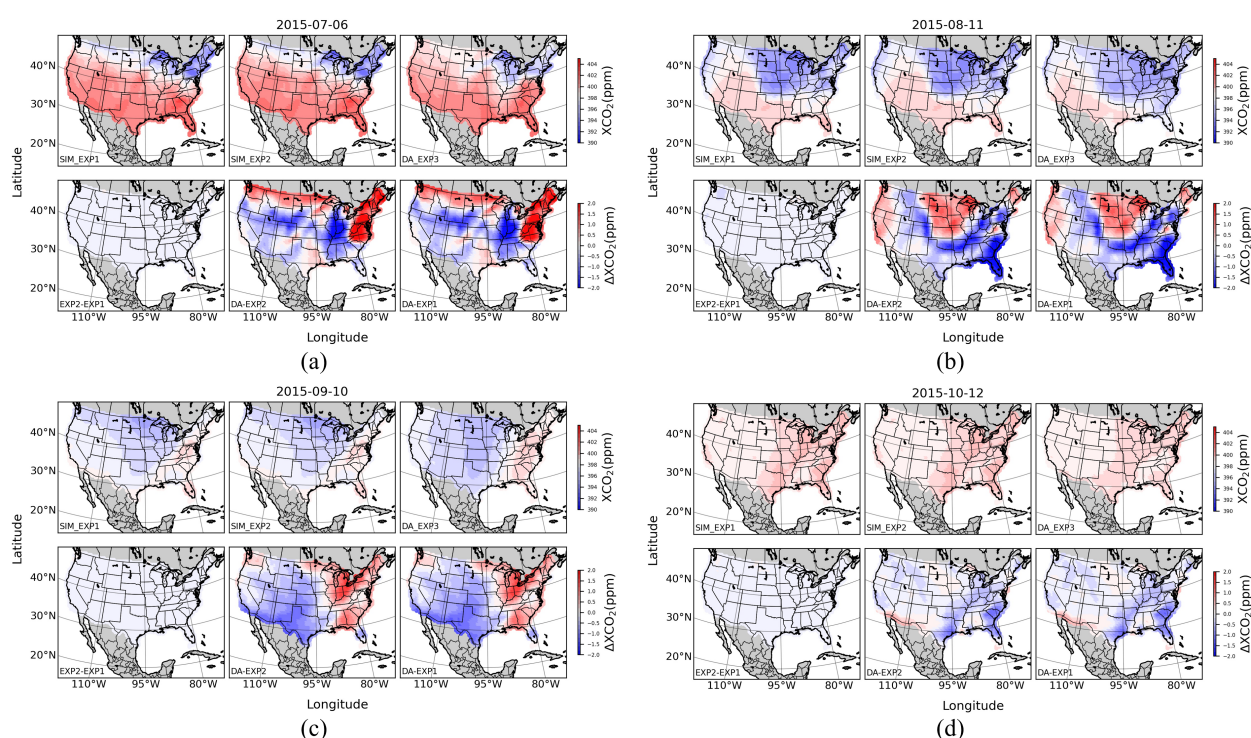

Figure 5. The spatial distribution of the daily XCO_2 (**upper panal**) and ΔXCO_2 (**lower panel**) of SIM_EXP1, SIM_EXP2 and DA_EXP3. **(a)** 6 July 2015; **(b)** 11 August 2015; **(c)** 10 September 2015; **(d)** 12 October 2015.

From 2016 to 2018, The selected spatial distribution of CT2019B wildfire CO_2 emissions, OCO-2 XCO_2 retrievals with nadir mode, the 10m wind speed and wind direction shows in Appendix A.

4. Conclusions

In this paper, we evaluate the wildfire CO_2 emissions in conterminous United States estimated by the regional CO_2 assimilation system with OCO-2 XCO_2 retrievals. The results is shown that the four-month (July to October) averaged wildfire CO_2 emissions in 2015-2018 are 4.408 Tg C, 1.784 Tg C, 1.514 Tg C, 2.873 Tg C respectively. The results are fall within one standard deviation of the estimates from CT2019B, FINNv1.5 and GFASv1.2, except for 2017, even though the wildfire CO_2 emissions has a big gap between different datasets in monthly. And the reason that the estimates of CO_2 emissions in 2017 has larger uncertainty is the lack of OCO-2 XCO_2 retrievals in August and September 2017.

The results indicate the potential of the regional carbon assimilation inversion system for estimating regional wildfire CO_2 emissions. However, due to the representiveness error of the observations, model error of the chemical transport model and assimilation algorithm, the results of this study still have uncertainty. It needs more works to improve the method for quantifying the wildfires CO_2 emissions more accurately.

Author Contributions: Conceptualization, Q.G.; methodology, J.J. and Q.Z.; software, J.J. and Q.Z.; validation, J.J.; formal analysis, J.J.; investigation, J.J.; resources, J.J.; data curation, J.J.; writing—original draft preparation, J.J. and Q.Z.; writing—review and editing, J.J., Y.H., C.W. and Q.G.; visualization, J.J.; supervision, Q.G.; project administration, J.J.; funding acquisition, Q.G. All authors have read and agreed to the published version of the manuscript.

Institutional Review Board Statement: Not applicable.

Informed Consent Statement: Not applicable.

Data Availability Statement: CT2019B data are provided by the National Oceanic and Atmospheric Administration (NOAA) and available from Global Monitoring Laboratory https://gml.noaa.gov/aftp/products/carbontracker/co2/CT2019B/ (accessed on 15 November 2023); OCO-2 V10 data are provied by NASA and available from EARTHDATA https://disc.gsfc.nasa.gov/datasets?keywords=OCO-2 (accessed on 15 November 2023); Meteorological data are provied by National Centers for Environmental Prediction (NCEP) and availible from http://database.rish.kyoto-u.ac.jp/arch/ncep/data/ncep.reanalysis2/gaussian_grid/ (accessed on 15 November 2023).

Conflicts of Interest: Author Qinwei Zhang was employed by the company Sungrow Power Shanghai Company Limited. The remaining authors declare that the research was conducted in the absence of any commercial or financial relationships that could be construed as a potential conflict of interest.
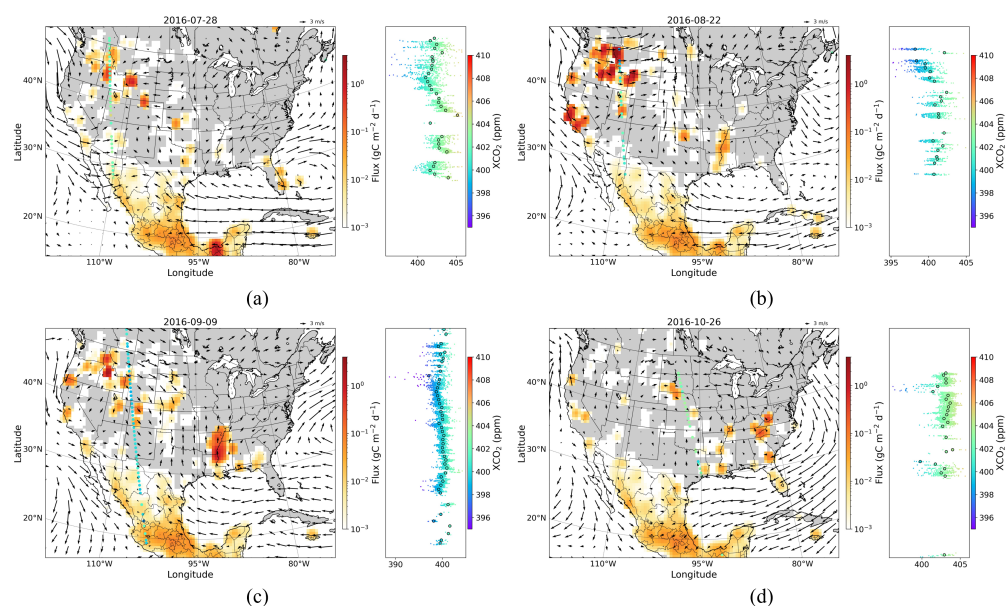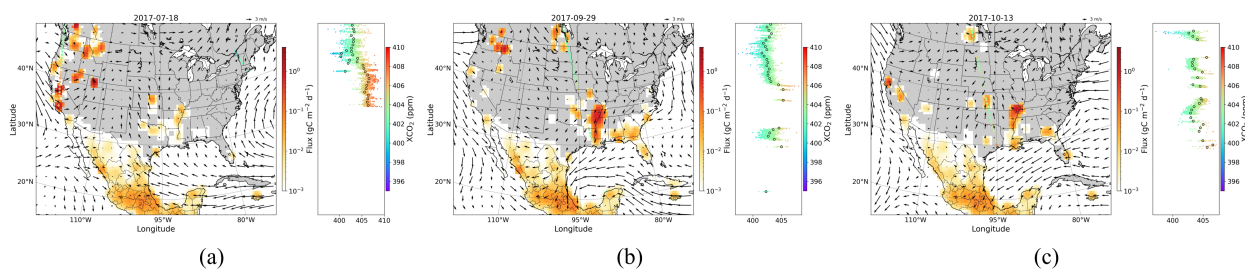
Appendix A

Figure A1. The spatial distribution of CT2019B wildfire CO_2 emissions with the 10m wind speed and wind direction, 10s average OCO-2 XCO$_2$ retrievals with nadir mode (**left panel**), the latitude variation of 10s average OCO-2 XCO$_2$ retrievals with nadir mode (**right panel**). (**a**) 28 July 2016; (**b**) 22 August 2016; (**c**) 9 September 2016; (**d**) 26 October 2016.

Figure A2. The spatial distribution of CT2019B wildfire CO_2 emissions with the 10m wind speed and wind direction, 10s average OCO-2 XCO_2 retrievals with nadir mode (**left panel**), the latitude variation of 10s average OCO-2 XCO_2 retrievals with nadir mode (**right panel**). **(a)** 18 July 2017; **(b)** 29 September 2017; **(c)** 13 October 2017.
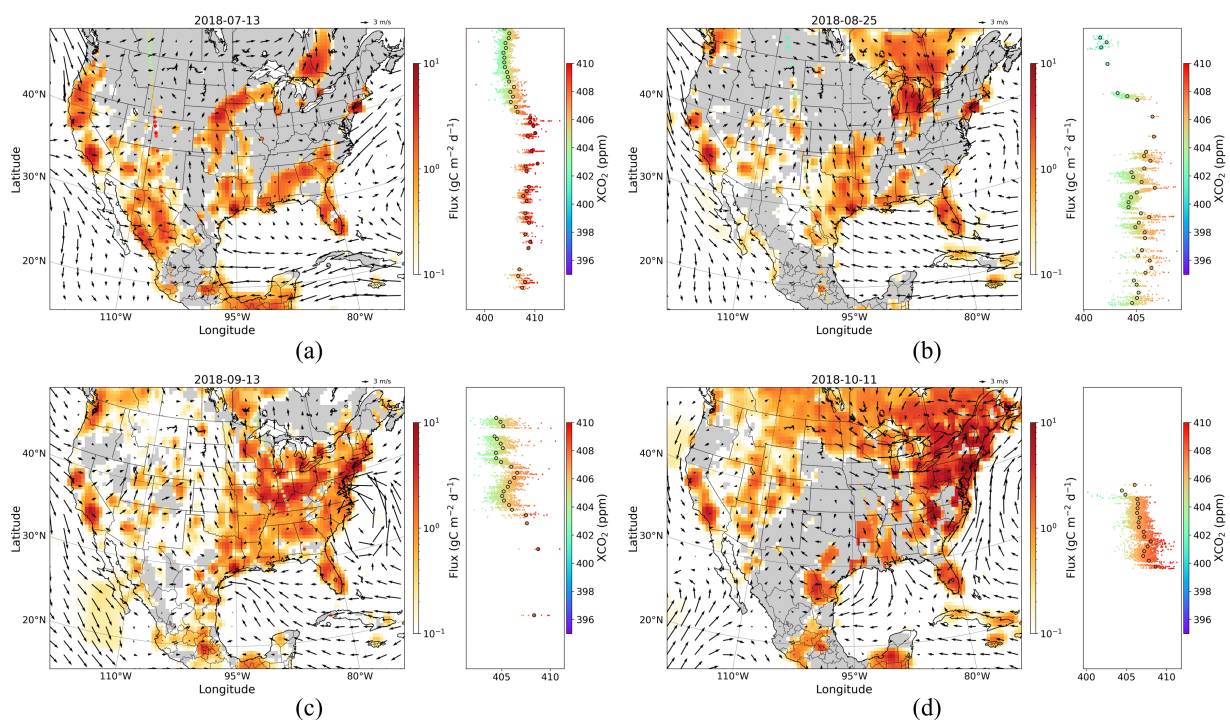

Figure A3. The spatial distribution of CT2019B wildfire CO_2 emissions with the 10m wind speed and wind direction, 10s average OCO-2 XCO_2 retrievals with nadir mode (**left panel**), the latitude variation of 10s average OCO-2 XCO_2 retrievals with nadir mode (**right panel**). **(a)** 13 July 2018; **(b)** 25 August 2018; **(c)** 13 September 2018; **(d)** 11 October 2018.

References

1. Andreae, M.O.; Merlet, P. Emission of trace gases and aerosols from biomass burning. *Glob. Biogeochem* **2001**, *15*, 955–966.
2. Change, I.C. Contribution of working groups I, II and III to the fourth assessment report of the intergovernmental panel on climate change. *Synthesis Report* **2007**.
3. Langmann, B.; Duncan, B.; Textor, C.; Trentmann, J.; van der Werf, G.R. Vegetation fire emissions and their impact on air pollution and climate. *Atmos. Environ.* **2009**, *43*, 107–116.
4. Jaffe, D.A.; Wigder, N.L. Ozone production from wildfires: A critical review. *Atmos. Environ.* **2012**, *51*, 1–10.
5. Bond, T.C.; Doherty, S.J.; Fahey, D.W.; Forster, P.M.; Berntsen, T.; DeAngelo, B.J.; Flanner, M.G.; Ghan, S.; Kärcher, B.; Koch, D.; et al. Bounding the role of black carbon in the climate system: A scientific assessment. *J. Geophys. Res. Atmos.* **2013**, *118*, 5380–5552.
6. Lorenz, K.; Lal, R., Introduction. In *Carbon Sequestration in Forest Ecosystems*; Springer Netherlands: Dordrecht, 2010; pp. 1–21.
7. Mead, M.I.; Castruccio, S.; Latif, M.T.; Nadzir, M.S.M.; Dominick, D.; Thota, A.; Crippa, P. Impact of the 2015 wildfires on Malaysian air quality and exposure: a comparative study of observed and modeled data. *Environ. Res. Lett.* **2018**, *13*, 044023.
8. Burke, M.; Driscoll, A.; Heft-Neal, S.; Xue, J.; Burney, J.; Wara, M. The changing risk and burden of wildfire in the United States. *Proc. Natl. Acad. Sci. USA* **2021**, *118*, e2011048118.

9.   Li, A.X.; Wang, Y.; Yung, Y.L. Inducing Factors and Impacts of the October 2017 California Wildfires. *Earth Space Sci.* **2019**, *6*, 1480–1488.

10. Rooney, B.; Wang, Y.; Jiang, J.H.; Zhao, B.; Zeng, Z.C.; Seinfeld, J.H. Air quality impact of the Northern California Camp Fire of November 2018. *Atmos. Chem. Phys.* **2020**, *20*, 14597–14616.

11. Wang, D.; Guan, D.; Zhu, S.; Kinnon, M.M.; Geng, G.; Zhang, Q.; Zheng, H.; Lei, T.; Shao, S.; Gong, P.; et al. Economic footprint of California wildfires in 2018. *Nat. Sustain.* **2021**, *4*, 252–260.

12. Zheng, B.; Ciais, P.; Chevallier, F.; Yang, H.; Canadell, J.G.; Chen, Y.; van der Velde, I.R.; Aben, I.; Chuvieco, E.; Davis, S.J.; et al. Record-high CO_2 emissions from boreal fires in 2021. *Science* **2023**, *379*, 912–917.

13. Bond-Lamberty, B.; Peckham, S.D.; Ahl, D.E.; Gower, S.T. Fire as the dominant driver of central Canadian boreal forest carbon balance. *Nature* **2007**, *450*, 89–92.

14. Rosa, I.M.D.; Pereira, J.M.C.; Tarantola, S. Atmospheric emissions from vegetation fires in Portugal (1990–2008): estimates, uncertainty analysis, and sensitivity analysis. *Atmos. Chem. Phys.* **2011**, *11*, 2625–2640.

15. Miranda, A.; Coutinho, M.; Borrego, C. Forest fire emissions in Portugal: A contribution to global warming? *Environ. Pollut.* **1994**, *83*, 121–123.

16. Shi, Y.; Yamaguchi, Y. A high-resolution and multi-year emissions inventory for biomass burning in Southeast Asia during 2001–2010. *Atmos. Environ.* **2014**, *98*, 8–16.

17. Ross, A.N.; Wooster, M.J.; Boesch, H.; Parker, R. First satellite measurements of carbon dioxide and methane emission ratios in wildfire plumes. *Geophys. Res. Lett.* **2013**, *40*, 4098–4102.

18. Ban, Y.; Zhang, P.; Nascetti, A.; Bevington, A.R.; Wulder, M.A. Near Real-Time Wildfire Progression Monitoring with Sentinel-1 SAR Time Series and Deep Learning. *Sci. Rep.* **2020**, *10*, 1322.

19. Liu, X.; He, B.; Quan, X.; Yebra, M.; Qiu, S.; Yin, C.; Liao, Z.; Zhang, H. Near Real-Time Extracting Wildfire Spread Rate from Himawari-8 Satellite Data. *Remote Sens.* **2018**, *10*.

20. Van Der Werf, G.R.; Randerson, J.T.; Giglio, L.; Van Leeuwen, T.T.; Chen, Y.; Rogers, B.M.; Mu, M.; Van Marle, M.J.E.; Morton, D.C.; Collatz, G.J.; et al. Global fire emissions estimates during 1997–2016. *Earth Syst. Sci. Data* **2017**, *9*, 697–720.

21. Van der Werf, G.R.; Randerson, J.T.; Giglio, L.; Collatz, G.J.; Mu, M.; Kasibhatla, P.S.; Morton, D.C.; DeFries, R.S.; Jin, Y.; Van Leeuwen, T.T. Global fire emissions and the contribution of deforestation, savanna, forest, agricultural, and peat fires (1997–2009). *Atmos. Chem. Phys.* **2010**, *10*, 11707–11735.

22. Wiedinmyer, C.; Akagi, S.K.; Yokelson, R.J.; Emmons, L.K.; Al-Saadi, J.A.; Orlando, J.J.; Soja, A.J. The Fire INventory from NCAR (FINN): a high resolution global model to estimate the emissions from open burning. *Geosci. Model Dev. Discuss.* **2011**, *4*, 625–641.

23. Kaiser, J.W.; Heil, A.; Andreae, M.O.; Benedetti, A.; Chubarova, N.; Jones, L.; Morcrette, J.J.; Razinger, M.; Schultz, M.G.; Suttie, M.; et al. Biomass burning emissions estimated with a global fire assimilation system based on observed fire radiative power. *Biogeosciences* **2012**, *9*, 527–554.

24. Konovalov, I.B.; Berezin, E.V.; Ciais, P.; Broquet, G.; Beekmann, M.; Hadji-Lazaro, J.; Clerbaux, C.; Andreae, M.O.; Kaiser, J.W.; Schulze, E.D. Constraining CO_2 emissions from open biomass burning by satellite observations of co-emitted species: a method and its application to wildfires in Siberia. *Atmos. Chem. Phys.* **2014**, *14*, 10383–10410.

25. Heymann, J.; Reuter, M.; Buchwitz, M.; Schneising, O.; Bovensmann, H.; Burrows, J.P.; Massart, S.; Kaiser, J.W.; Crisp, D. CO_2 emission of Indonesian fires in 2015 estimated from satellite-derived atmospheric CO_2 concentrations. *Geophys. Res. Lett.* **2017**, *44*, 1537–1544.

26. Guo, M.; Li, J.; Xu, J.; Wang, X.; He, H.; Wu, L. CO_2 emissions from the 2010 Russian wildfires using GOSAT data. *Environmental Pollution* **2017**, *226*, 60–68.

27. Guo, B.; Li.; Wen.; Huang, R. Estimation of CO_2 Emissions from Wildfires Using OCO-2 Data. *Atmosphere* **2019**, *10*, 581.

28. Wang, J.; Liu, Z.; Zeng, N.; Jiang, F.; Wang, H.; Ju, W. Spaceborne detection of XCO_2 enhancement induced by Australian mega-bushfires. *Environ. Res. Lett.* **2020**, *15*, 124069.

29. Zhang, Q.; Li, M.; Wei, C.; Mizzi, A.P.; Huang, Y.; Gu, Q. Assimilation of OCO-2 retrievals with WRF-Chem/DART: A case study for the Midwestern United States. *Atmos. Environ.* **2021**, *246*, 118106.

30. Anderson, J.; Hoar, T.; Raeder, K.; Liu, H.; Collins, N.; Torn, R.; Avellano, A. The Data Assimilation Research Testbed: A Community Facility. *Bull. Am. Meteorol. Soc.* **2009**, *90*, 1283 – 1296.

31. Hong, S.Y.; Dudhia, J.; Chen, S.H. A Revised Approach to Ice Microphysical Processes for the Bulk Parameterization of Clouds and Precipitation. *Mon. Weather. Rev.* **2004**, *132*, 103 – 120.

32. Kain, J.S. The Kain–Fritsch Convective Parameterization: An Update. *J. Appl. Meteorol.* **2004**, *43*, 170 – 181.

33. Mlawer, E.J.; Taubman, S.J.; Brown, P.D.; Iacono, M.J.; Clough, S.A. Radiative transfer for inhomogeneous atmospheres: RRTM, a validated correlated-k model for the longwave. *J. Geophys. Res. Atmos.* **1997**, *102*, 16663–16682.

34. Dudhia, J. Numerical Study of Convection Observed during the Winter Monsoon Experiment Using a Mesoscale Two-Dimensional Model. *J. Atmos. Sci.* **1989**, *46*, 3077 – 3107.

35. Gerrity, J.P.; Black, T.L.; Treadon, R.E. The Numerical Solution of the Mellor-Yamada Level 2.5 Turbulent Kinetic Energy Equation in the Eta Model. *Mon. Weather. Rev.* **1994**, *122*, 1640 – 1646.

36. Nakanishi, M.; Niino, H. Development of an Improved Turbulence Closure Model for the Atmospheric Boundary Layer. *J. Meteorol. Soc. Jpn. Ser. II* **2009**, *87*, 895–912.

37. Crowell, S.; Baker, D.; Schuh, A.; Basu, S.; Jacobson, A.R.; Chevallier, F.; Liu, J.; Deng, F.; Feng, L.; McKain, K.; et al. The 2015–2016 carbon cycle as seen from OCO-2 and the global in situ network. *Atmos. Chem. Phys.* **2019**, *19*, 9797–9831.

38. Anderson, J.L. A Local Least Squares Framework for Ensemble Filtering. *Mon. Weather. Rev.* **2003**, *131*, 634 – 642.

39. Mizzi, A.P.; Arellano Jr., A.F.; Edwards, D.P.; Anderson, J.L.; Pfister, G.G. Assimilating compact phase space retrievals of atmospheric composition with WRF-Chem/DART: a regional chemical transport/ensemble Kalman filter data assimilation system. *Geosci. Model Dev.* **2016**, *9*, 965–978.

40. Anderson, J.L. Localization and Sampling Error Correction in Ensemble Kalman Filter Data Assimilation. *Mon. Weather. Rev.* **2012**, *140*, 2359 – 2371.

41. Hakkarainen, J.; Ialongo, I.; Tamminen, J. Direct space-based observations of anthropogenic CO_2 emission areas from OCO-2. *Geophys. Res. Lett.* **2016**, *43*, 11,400–11,406.

42. Hakkarainen, J.; Ialongo, I.; Maksyutov, S.; Crisp, D. Analysis of Four Years of Global XCO_2 Anomalies as Seen by Orbiting Carbon Observatory-2. *Remote Sens.* **2019**, *11*.

43. Anderson, J.L. An Ensemble Adjustment Kalman Filter for Data Assimilation. *Mon. Weather. Rev.* **2001**, *129*, 2884 – 2903.

44. Gaspari, G.; Cohn, S.E. Construction of correlation functions in two and three dimensions. *Q. J. R. Meteorol. Soc.* **1999**, *125*, 723–757.

45. Kang, J.S.; Kalnay, E.; Miyoshi, T.; Liu, J.; Fung, I. Estimation of surface carbon fluxes with an advanced data assimilation methodology. *J. Geophys. Res. Atmos.* **2012**, *117*.

46. CAMS global biomass burning emissions based on fire radiative power (GFAS): data documentation. https://confluence.ecmwf.int/display/CKB/CAMS+global+biomass+burning+emissions+based+on+fire+radiative+power+%28GFAS%29%3A+data+documentation. Accessed on 15 November 2023.

47. Marlier, M.E.; Voulgarakis, A.; Shindell, D.T.; Faluvegi, G.; Henry, C.L.; Randerson, J.T. The role of temporal evolution in modeling atmospheric emissions from tropical fires. *Atmos. Environ.* **2014**, *89*, 158–168.